# Tectonic setting and source of the NW–SE trending mafic dykes from the Tikamgarh area, Bundelkhand craton

R. Sreenivas[1], M. Srinivas[1], Ch. Karunakar[1] and A. Ajay Kumar[1]
[1]*Department of Geology, Osmania University, Hyderabad-500007*

***Abstract*- In this study, we present the geochemical analysis of distinct NW–SE trending mafic dykes from Tikamgarh area, Bundelkhand craton. These dykes have not been studied previously and highlight the importance of igneous and tectonic processes in the Tikamgarh area, Bundelkhand craton. These dykes are characterised as basaltic nature (SiO2 = 48.8–50.0 wt.%; Mg# = 44.10–61.2), and comparable with MORB type tholeiitic magma series. The LREE is enriched, and the HREE is almost flat in Tikamgarh samples, with $La_N/Sm_N$ ratios (1.3-1.6), and $Sm_N/Lu_N$ ratios (0.8-1.5), which likely suggests that they originated from distinct mantle melts. The $TiO_2$/Yb vs. Nb/Yb plot reveals the melting depth at which variations reflect spinel residue source, which has a shallower melting temperature with spinel. The dyke magmas inherited variably enriched compositions as a result of interaction of upwelling mantle melts with metasomatised subcontinental lithospheric mantle.**

**Keywords: mafic dykes; geochemistry; source; tectonic setting.**

## I. INTRODUCTION

Mafic dykes trending NW-SE directions are recognized in the Tikamgarh area, Bundelkhand craton, which are dominant the area. Although multiple authors, based on geochemistry have concluded that the NW-SE trending dykes of Bundelkhand were emplaced in multiple magmatic pulses of more than one generation [1]. Hence, it is apparent that the NW-SE trending mafic dykes of Bundelkhand craton were emplaced in multiple magmatic pulses. This study presents source and tectonic setting of Tikamgarh NW-SE trending dykes. Here, we provide major and trace element geochemistry of the NW-SE trending mafic dykes. The geochemical data is used to identify and evaluate the role of source and tectonic setting to understand the observed compositional variations of the dykes. Finally, we propose a detailed account regarding the petrogenesis of geochemically distinct groups of NW-SE trending dykes.

## II. THE GEOLOGY AND FIELD OF THE STUDY AREA

The Bundelkhand craton forms the northern block of the Indian Shield. The southern section of the Indian Shield is one of the components. The research region is situated inside the quasi-triangular Bundelkhand craton. The sedimentary and volcanic elements that date back to the Paleoproterozoic era are exposed along the basin borders in both the southern and northern parts of the Gwalior and Bijawar basins. The Mesoproterozoic Vindhyan basin may be found in an area that is directly above the craton's southern and southeastern edges [2]–[4]. Recent studies using Pb-Pb and U-Pb dating on basement gneiss zircons have yielded significantly younger ages, such as an ion microprobe $^{207}Pb/^{206}Pb$ age of 3270± 3 Ma [5] and a SIMS U-Pb age of 3301±2Ma [6]. Two E-W trending lineaments, in addition to the TTGs, make the metasedimentary and metavolcanic rocks of the greenschist to lower amphibolite facies [7]. The preponderance of the craton is made up of the Bundelkhand Granitoid Complex. Granodiorites, Syeno- and monzogranites, granite porphyries, alkali feldspar syenites, and diorites are all part of the granitoid complex [5], [8].

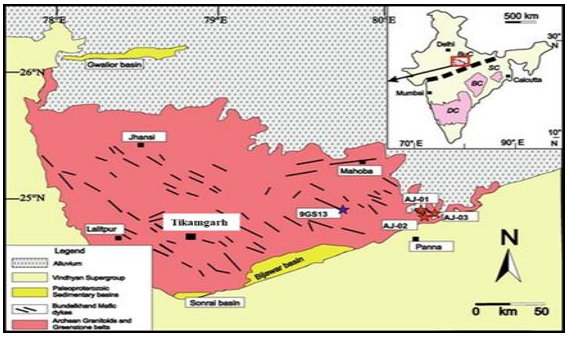


Figure 1: The geological map shown depicts a section of the Bundelkhand Craton, highlighting prominent lithologic units alongside the Tikamgarh mafic dykes that have been subject to study.


Figure 2: Photographs from the field depicting mafic dykes discovered near the Chapra area (a) Mafic dyke injected into pink granite exposed east of Chapra area; (b) Coarse to medium-grained mafic dyke with small felsic-injection and associated with host pink granite exposed northeast of Chapra area.


Figure 3: Photographs from the field depicting mafic dykes discovered near Gangchari and Tisgina areas (a) Mafic dyke exposed as large boulders east of Gangchari area; (b) Medium to fine-grained mafic dyke exposed as huge mafic boulders east of Tisgina area.

Mafic dykes with a sparser population with ENE-WSW and a dense network of NW-SE as well as NE-SW trending dykes cutting across all exposed lithologies are the main features of the Bundelkhand craton's most recent magmatic activity. These dykes typically have a grain size ranging from medium to coarse, are primarily unaltered, and have a sharp chilled contact with the rocks they cut throughout. These are exposed as a sequence of linear and discontinuous outcrops that range in length from a few meters to twenty kilometers.

Tikamgarh, located around 60 kilometers to the south-southeast of the Jhansi, was another significant location covered during this project. This area is widely exposed with mafic dykes running NW to SE; trending dykes are also present (Figure 2). The dyke length ranges from a few meters to a few kilometers. In a few areas, dioritic-composed mafic dykes are also encountered; this is believed to be the result of differentiation. Most dykes produce linear ridges with boulder outcrops and intrude into granitoids (Figure 3).

## III. PETROGRAPHY

The Tikamgarh mafic dykes, which exhibit a northwest-to-southeast orientation, are mostly characterised by a medium to coarse-grained texture. However, a small number of fine-grained samples have been observed at the margins of the dykes. Plagioclase and clinopyroxene, mostly augite, are observed in medium- to coarse-grained form in many thin sections (Figures 4 and 5). The samples under study have a distinctive ophitic or sub-ophitic texture, whereby augite grains with plagioclase laths are frequently observed. Within this particular region, there is evidence of deformed plagioclase exhibiting lamellar twinning, characterised by the presence of fracture-filled mafic mineral (as seen in Figure 4a). The subhedral grains of augite undergo alteration to chlorite, shown in Figure 5b, along with twinned plagioclase, as represented in Figure 4b. Frequently, plagioclase grains undergo alterations resulting in saussuritisation and sericitization, shown in Figure 5a. The majority of thin sections often include apatite, zircon/baddeleyite, ilmenite/magnetite, and titanite as accessory minerals. The samples may be classified as dolerite and meta-dolerite based on their mineralogical and textural properties.

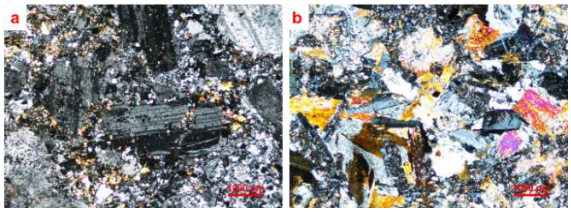


**Figure 4:** (a) deformed plagioclase shows lamellar twinning where fracture-filled mafic mineral. (b) Subhedral grains of augite grain alters to chlorite.

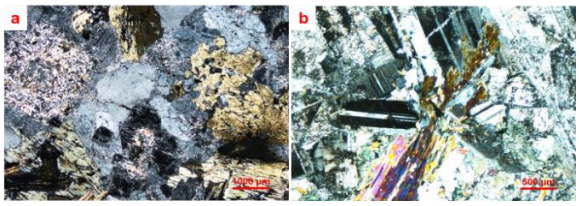


**Figure 5:** (a) Photograph of plagioclase altered to saussuritisation and sericitisation associated with hornblende and biotite (XPL). (b) augite transformed into chlorite associated with twinned plagioclase (XPL).

## IV. RESULTS AND DISCUSSION

The studied rocks are classified based on the most popular classification diagrams: IUGS recommended Total alkalis – silica (TAS) diagram [9], [10], (ii) Classification based on Nb/Y and Zr/Ti ratios [11]. Total alkali-silica (TAS) is the IUGS-recommended and most common classification for igneous materials.

It was initially established by [12], with modifications made by the IUGS sub-commission on "Systematic of Igneous Rocks" [10], [13]. The plot displays most of the examined samples demonstrating sub-alkaline geochemical attributes and displaying a basaltic composition (Figure 6a). The classification diagram based on high-field strength elements (HFSE) (see Figure 6b) also corroborates basalt characteristics; after [11].

Tikamgarh dykes have a flat REE pattern ($(La/Yb)_{CN}$ = 1.2 to 1.9; subscript CN signifies chondrite normalised value), with the majority of samples exhibiting a modest positive Eu anomaly ($Eu^* = Eu_{CN}/(Sm_{CN}*Gd_{CN})$ = 1.1 to 1.2, Table 2) (Figure 7a). Tikamgarh samples had the least LREE to HREE fractionation ($(La/Yb)_{CN}$ = 1.2 to 1.9). Tikamgarh dykes have noticeable fractionation in LREE and lower $(La/Sm)_{CN}$ values (1.2 to 1.7). In primordial mantle normalised multi-element spidergrams, the majority of examined dykes from all three groups exhibit negative Nb anomaly ($Nb^* = Nb_{PM}/(Th_{PM}*La_{PM})$; (subscript PM represents primordial mantle normalised value) (Figure 7b). Sr and Ti exhibit prominently positive anomalies in Tikamgarh samples.

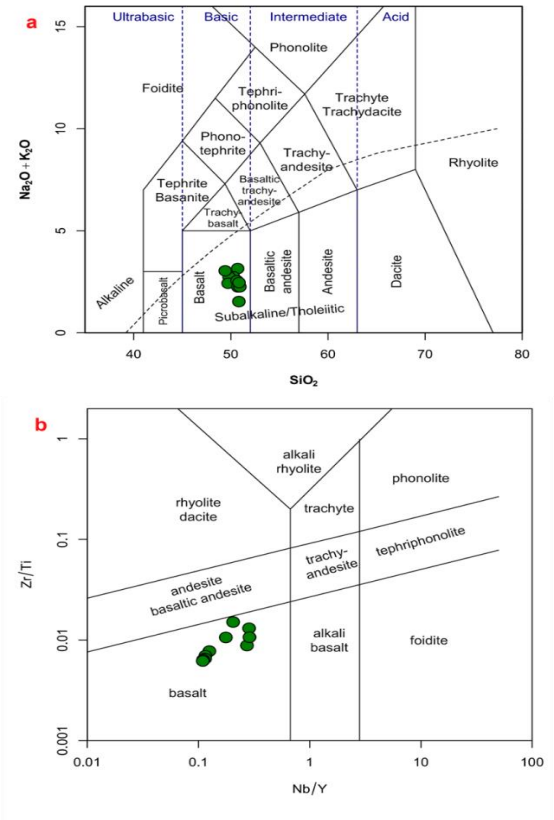


Figure 6: (a) Total alkalis and silica (TAS) classification plot (following Le Maitre et al., 2002). It also distinguishes between sub-alkaline and alkaline basalts, as shown by the dashed line (after Irvine and Baragar, 1971). (b) Classification diagrams based on the ratios of Nb/Y and Zr/Ti are used ( J. A. Winchester and P. A. Floyd).

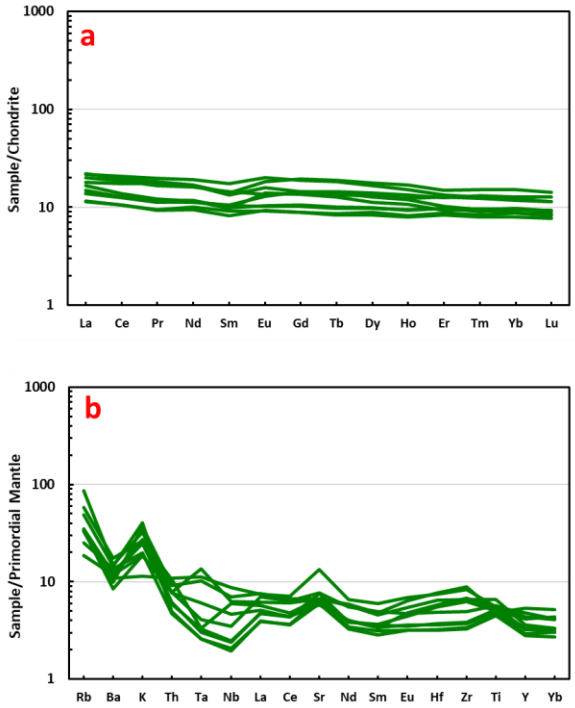


**Figure 7. (a)** The figures shown are a chondrite-normalized rare-earth element (REE) diagram. The chondrite values used in this study were sourced from a (Nakamura 1974). **(b)** The multi-element spidergrams shown are normalised to the primitive mantle. The parameters for the primordial mantle were obtained from the study conducted by (McDonough,1992).

The $La_N/Sm_N$, $La_N/Lu_N$, and $Sm_N/Lu_N$ ratios are compared (Figure 8a,b) to verify this difference. The REE patterns were flat in the samples we looked at Tikamgarh dykes, the $La_N/Sm_N$, $La_N/Lu_N$, and $Sm_N/Lu_N$ ratios are close to 2. The LREE is enriched, and the HREE is almost flat in Tikamgarh dyke samples, with $La_N/Sm_N$ ratios (1.3-1.6), and $Sm_N/Lu_N$ ratios (0.8-1.5), respectively. On the $La_N$ vs. $Sm_N$ (Figure 8a), $Sm_N$ vs. $Lu_N$ (Figure 8b) plots, the distinctive REE properties of Tikamgarh samples. This likely suggests that they originated from distinct mantle melts. The presence or absence of residual

garnet inside the mantle source might impact the $Gd_{CN}/Yb_{CN}$ ratios seen in the samples, providing insights into a degree of partial melting occurring at the source depth that subsequently gives rise to the formation of dykes. In the $(Gd/Yb)_M$ vs. $(La/Yb)_M$ diagram, the Tikamgarh dykes obviously plot in the spinel stability field (Figure 9a, M stands for primitive normalised). This occurrence implies that the formation of dykes may be attributed to the mantle melting process, namely involving the melting of the spine-rich mantle. The low range Dy/Yb ratio of Tikamgarh dyke samples may be associated with an enriched source and magma's origin from the spinel lherzolite mantle zone (Davidson et al., 2013). The $TiO_2$/Yb vs. Nb/Yb plot (Figure 9b) reveals the melting depth at which variations in $TiO_2$/Yb and Nb/Yb reflect spinel residue source, respectively (Pearce, 2008). E-MORB is distinguished from OIB by its deeper melting with garnet residues, while E-MORB has a shallower melting temperature with spinel (Figure 9b). The preponderance of samples is, therefore, compatible with shallower melting.

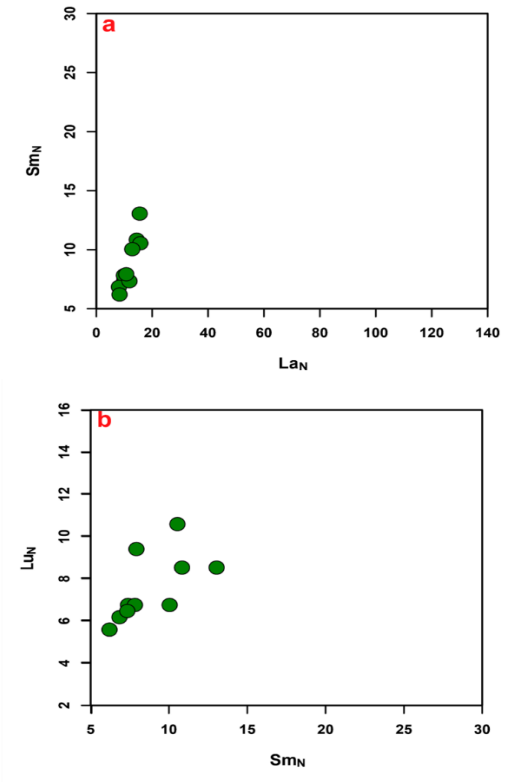


Figure 8: (a) $La_N$ vs. $Sm_N$, and (b) $Sm_N$ vs. $Lu_N$ variation plots for mafic dykes from Tikamgarh. Chondrite values were derived from Nakamura, (1974).

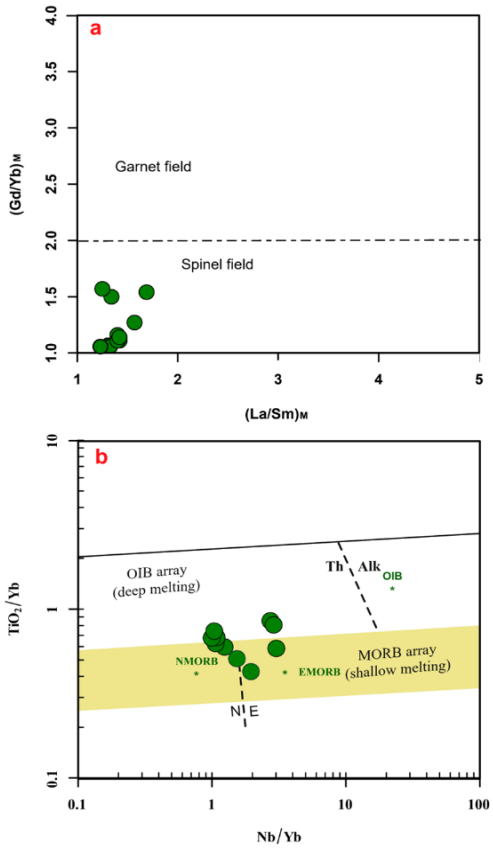


Figure 9: (a) The $(Gd/Yb)_M$ versus $(La/Sm)_M$ variation diagram distinguishes between spinel and garnet mantle sources.. (M = Primitive normalised). (b) The diagram by Pearce (2008) evaluates the depth of melting between $TiO_2$/Yb and Nb/Yb.

The geochemistry indicates similar mantle sources, similar genesis and magmatic evolution for the Tikamgarh dykes suggest their derivation under the same set of mantle conditions. The majority of these samples, which are basalts to basaltic nature, are found within the continental tholeiitic to calc-alkaline basaltic regions (Figure 10a) [18]. These dykes are suggestive of plume-induced formations that exhibit characteristics associated with a previous subduction event. To facilitate a more comprehensive analysis, we used triangle discrimination diagrams, namely Nb*2 vs Zr/4 versus Y (Figure 10b) that provided insights into the tectonic environments in which the mafic dykes under investigation were formed. These diagrams were adopted from[19], [20], , respectively. In both figures, the samples are seen to plot either inside the basaltic field associated with the tectonic plate or as arc basalts.

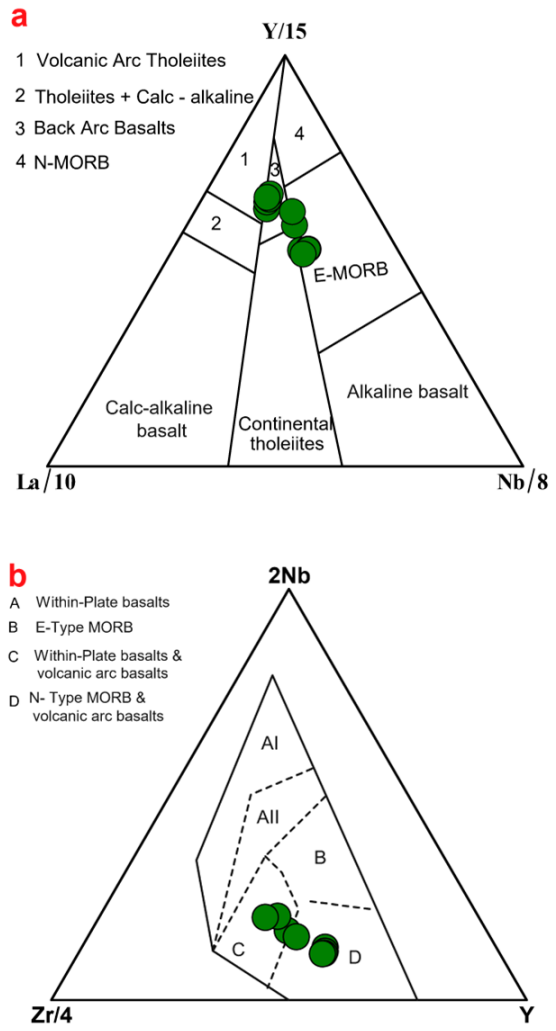


Figure 10: Discrimination diagrams are shown for the purpose of differentiating various tectonic settings. (a) depicts a triangle diagram, known as the La/10–Y/15–Nb/8 diagram, which is used for the discriminating of tectonic settings. (Cabanis and Lecolle, 1989). (b) Zr–Nb–Y tectonic plot (after Meschede, 1986). Rollinson, (2014) delineated the domains including arc basalts, MORB, continental flood basalts, as well as ocean-island and alkali basalts, as per the findings reported by Shervais, (1982).

## V. CONCLUSIONS

NW-SE trending of Tikamgarh mafic dyke intrusions constitute important igneous activity of the Bundelkhand Craton, India. Major and trace element geochemistry suggests that the dykes are iron rich subalkalic continental tholeiites. In Tikamgarh samples, the LREE is enriched, but the HREE is practically flat, indicating that they originated from different mantle melts. The $TiO_2$/Yb vs. Nb/Yb figure shows the melting depth at which differences reflect the source of the spinel residue, which has a shallower melting temperature. As a result of the interaction of upwelling mantle melts with metasomatised subcontinental lithospheric mantle, the dyke magmas inherited a variety of enriched compositions.

Table 1 Major oxide data of mafic dykes trending in the NW-SE direction of the Tikamgarh area, Bundelkhand craton.

| S No. | T6 | T7 | T8 | T9 | T21 | JL27 | JL28A | JL29 | JL36 | JL37 |
|---|---|---|---|---|---|---|---|---|---|---|
| $SiO_2$ | 50.00 | 49.50 | 49.10 | 48.80 | 49.20 | 49.60 | 49.70 | 49.80 | 49.80 | 49.60 |
| $Al_2O_3$ | 12.50 | 12.20 | 11.50 | 12.30 | 12.10 | 11.90 | 10.70 | 10.30 | 11.30 | 11.80 |
| $Fe_2O_3$ | 17.20 | 13.00 | 13.40 | 12.80 | 13.50 | 12.00 | 13.50 | 12.70 | 12.30 | 12.00 |
| MnO | 0.16 | 0.16 | 0.16 | 0.16 | 0.16 | 0.13 | 0.15 | 0.14 | 0.13 | 0.13 |
| MgO | 6.20 | 7.80 | 8.50 | 9.20 | 8.30 | 7.90 | 7.20 | 8.10 | 7.60 | 7.70 |
| CaO | 8.10 | 12.00 | 12.00 | 11.40 | 12.20 | 12.70 | 13.00 | 14.10 | 13.10 | 12.70 |
| $Na_2O$ | 2.50 | 1.90 | 2.00 | 1.80 | 1.80 | 1.40 | 1.60 | 1.20 | 1.40 | 1.40 |
| $K_2O$ | 0.60 | 0.80 | 0.70 | 1.20 | 0.60 | 1.10 | 0.60 | 0.30 | 0.80 | 1.00 |
| $TiO_2$ | 1.20 | 1.00 | 1.10 | 1.00 | 1.00 | 1.10 | 1.40 | 1.20 | 1.20 | 1.10 |
| $P_2O_5$ | 0.14 | 0.10 | 0.10 | 0.09 | 0.09 | 0.13 | 0.15 | 0.12 | 0.14 | 0.12 |
| LOI | 1.40 | 1.50 | 1.30 | 1.30 | 1.10 | 2.20 | 2.00 | 1.90 | 2.30 | 2.60 |
| Total | 100 | 100 | 100 | 100 | 100 | 100 | 100 | 100 | 100 | 100 |
| Mg# | 44.10 | 56.90 | 58.00 | 61.20 | 57.50 | 59.20 | 54.10 | 58.50 | 57.60 | 58.40 |

Table 2 Trace and rare earth element data of mafic dykes with a northwest-southeast orientation of Tikamgarh area, Bundelkhand craton.

| S No. | T6 | T7 | T8 | T9 | T21 | JL27 | JL28A | JL29 | JL36 | JL37 |
|---|---|---|---|---|---|---|---|---|---|---|
| Sc | 25.37 | 30.55 | 30.13 | 30.89 | 29.23 | 25.78 | 24.34 | 27.05 | 33.41 | 28.81 |
| V | 182.09 | 185.4 | 188.41 | 177.32 | 172.38 | 98.87 | 99.29 | 98.55 | 74.86 | 71.9 |
| Cr | 62.58 | 98.62 | 105.48 | 112.37 | 93.54 | 100.45 | 169.52 | 134.06 | 125.23 | 91.26 |
| Co | 33.35 | 36.68 | 36.65 | 36.12 | 37.78 | 47.74 | 44.31 | 42.19 | 39.67 | 43.04 |
| Ni | 55.78 | 68.02 | 66.4 | 67.22 | 68.43 | 91.05 | 122.87 | 86.9 | 98.13 | 78.44 |
| Cu | 69.39 | 94.36 | 92.85 | 88.81 | 85.18 | 94.18 | 84.02 | 75.54 | 71.6 | 95.72 |
| Zn | 161.46 | 140.89 | 101.39 | 110.62 | 90.3 | 67.37 | 56.33 | 79.95 | 47.79 | 74.57 |
| Ga | 13.62 | 11.05 | 10.89 | 10.43 | 11.11 | 9.72 | 8.89 | 10.22 | 7.4 | 7.36 |
| Rb | 11.89 | 22.32 | 21.55 | 31.05 | 15.88 | 20.99 | 21.58 | 21.9 | 36.87 | 55.02 |
| Sr | 162.07 | 123.1 | 136.83 | 138.92 | 127.06 | 141.08 | 140.87 | 280.32 | 141.07 | 159.2 |
| Y | 19.83 | 14.71 | 15.23 | 13.32 | 12.75 | 24.46 | 16.36 | 21.63 | 14.89 | 18.76 |
| Zr | 55.75 | 41.74 | 42.99 | 38.03 | 37.01 | 99.47 | 73.78 | 93.88 | 76.52 | 69.71 |
| Nb | 2.49 | 1.7 | 1.75 | 1.47 | 1.4 | 5.03 | 4.47 | 6.19 | 4.29 | 3.31 |
| Cs | 0.33 | 0.61 | 0.51 | 0.48 | 0.56 | 0.92 | 0.61 | 0.27 | 0.7 | 0.46 |
| Ba | 82.41 | 84.56 | 84.35 | 101.4 | 95.29 | 69.01 | 59.04 | 76.25 | 121.45 | 103.6 |
| La | 4.77 | 3.3 | 3.26 | 2.68 | 2.74 | 5.19 | 4.24 | 5.12 | 3.91 | 3.53 |
| Ce | 11.25 | 7.82 | 7.69 | 6.47 | 6.4 | 11.85 | 10.69 | 12.6 | 8.47 | 7.74 |
| Pr | 1.57 | 1.09 | 1.06 | 0.89 | 0.88 | 1.74 | 1.65 | 1.88 | 1.15 | 1.08 |
| Nd | 7.53 | 5.49 | 5.32 | 4.67 | 4.41 | 7.92 | 7.73 | 8.94 | 5.38 | 5.2 |
| Sm | 2.2 | 1.5 | 1.59 | 1.39 | 1.26 | 2.14 | 2.04 | 2.65 | 1.49 | 1.61 |

| | | | | | | | | | | |
|---|---|---|---|---|---|---|---|---|---|---|
| **Eu** | 0.79 | 0.61 | 0.59 | 0.53 | 0.54 | 1.07 | 0.91 | 1.16 | 0.8 | 0.75 |
| **Gd** | 2.83 | 2.15 | 2.08 | 1.82 | 1.81 | 3.97 | 2.98 | 3.89 | 2.78 | 2.97 |
| **Tb** | 0.5 | 0.37 | 0.36 | 0.32 | 0.31 | 0.7 | 0.52 | 0.68 | 0.47 | 0.54 |
| **Dy** | 3.35 | 2.51 | 2.47 | 2.25 | 2.1 | 4.51 | 3.24 | 4.24 | 2.85 | 3.53 |
| **Ho** | 0.69 | 0.52 | 0.53 | 0.46 | 0.45 | 0.95 | 0.67 | 0.86 | 0.6 | 0.75 |
| **Er** | 2.11 | 1.6 | 1.61 | 1.44 | 1.37 | 2.45 | 1.68 | 2.2 | 1.53 | 2.08 |
| **Tm** | 0.31 | 0.23 | 0.24 | 0.21 | 0.2 | 0.39 | 0.24 | 0.32 | 0.24 | 0.33 |
| **Yb** | 2.01 | 1.6 | 1.62 | 1.48 | 1.35 | 2.58 | 1.64 | 2.05 | 1.49 | 2.16 |
| **Lu** | 0.29 | 0.23 | 0.23 | 0.21 | 0.19 | 0.36 | 0.23 | 0.29 | 0.22 | 0.32 |
| **Hf** | 1.51 | 1.11 | 1.16 | 0.99 | 0.98 | 2.37 | 2 | 2.32 | 1.8 | 1.71 |
| **Ta** | 0.17 | 0.12 | 0.13 | 0.11 | 0.11 | 0.42 | 0.56 | 0.46 | 0.14 | 0.25 |
| **Pb** | 2.14 | 1.58 | 1.24 | 1.16 | 2.62 | 2.12 | 2.46 | 4.02 | 2.04 | 2.52 |
| **Th** | 0.67 | 0.53 | 0.5 | 0.42 | 0.4 | 0.78 | 0.67 | 0.92 | 0.89 | 0.65 |
| **U** | 0.16 | 0.13 | 0.11 | 0.11 | 0.1 | 0.25 | 0.24 | 0.32 | 0.39 | 0.31 |
| **Rb/Sr** | 0.07 | 0.18 | 0.16 | 0.22 | 0.12 | 0.15 | 0.15 | 0.08 | 0.26 | 0.35 |
| **Zr/Y** | 2.81 | 2.84 | 2.82 | 2.86 | 2.9 | 4.07 | 4.51 | 4.34 | 5.14 | 3.72 |
| **Y/Nb** | 7.98 | 8.64 | 8.69 | 9.04 | 9.14 | 4.87 | 3.66 | 3.5 | 3.47 | 5.67 |
| **(La/Yb)$_{CN}$** | 1.7 | 1.48 | 1.44 | 1.3 | 1.46 | 1.44 | 1.85 | 1.79 | 1.88 | 1.17 |
| **(Ce/Sm)$_{CN}$** | 1.28 | 1.3 | 1.21 | 1.16 | 1.27 | 1.38 | 1.31 | 1.19 | 1.42 | 1.2 |
| **(Tb/Yb)$_{CN}$** | 1.4 | 1.42 | 1.32 | 1.25 | 1.4 | 1.56 | 1.34 | 1.25 | 1.69 | 1.41 |
| **(Gd/Yb)$_{PM}$** | 1.16 | 1.11 | 1.06 | 1.01 | 1.11 | 1.28 | 1.5 | 1.57 | 1.54 | 1.14 |
| **Eu*** | 0.97 | 1.03 | 0.99 | 1.02 | 1.09 | 1.12 | 1.13 | 1.1 | 1.21 | 1.04 |
| **Nb*** | 0.47 | 0.44 | 0.46 | 0.47 | 0.45 | 0.85 | 0.9 | 0.97 | 0.78 | 0.74 |
| **Nb/Yb** | 1.24 | 1.07 | 1.08 | 0.99 | 1.04 | 1.95 | 2.72 | 3.02 | 2.88 | 1.53 |
| **Th/Yb** | 0.33 | 0.33 | 0.31 | 0.28 | 0.3 | 0.3 | 0.41 | 0.45 | 0.6 | 0.3 |
| **Th/La** | 0.14 | 0.16 | 0.15 | 0.16 | 0.15 | 0.15 | 0.16 | 0.18 | 0.23 | 0.19 |
| **Nb/La** | 0.52 | 0.52 | 0.54 | 0.55 | 0.51 | 0.97 | 1.06 | 1.21 | 1.1 | 0.94 |
| **Nb/Ce** | 0.22 | 0.22 | 0.23 | 0.23 | 0.22 | 0.42 | 0.42 | 0.49 | 0.51 | 0.43 |
| **Rb/Y** | 0.6 | 1.52 | 1.41 | 2.33 | 1.25 | 0.86 | 1.32 | 1.01 | 2.48 | 2.93 |


## ACKNOWLEDGMENT

The authors thank the Head of the Department of Geology, Osmania University (Hyderabad). This work forms a part of the first author's Ph.D. thesis. We acknowledge to Dr. D Srinivasa Sarma, Chief Scientist CSIR-NGRI, Hyderabad, for his suggestions throughout the manuscript. We also thank to Dr. M. Ram Mohan, Chief Scientist and Dr. Keshava Krishna, Principal Scientist CSIR-NGRI, Hyderabad, for their help with ICP-MS and XRF analysis.


## REFERENCES


[1] B. P. Radhakrishna and S. M. Naqvi, "Precambrian continental crust of India and its evolution.," *J. Geol.*, vol. 94, no. 2, pp. 145–166, 1986, doi: 10.1086/629020.

[2] J. G. Meert, M. K. Pandit, V. R. Pradhan, and G. Kamenov, "Preliminary report on the paleomagnetism of 1.88 Ga dykes from the Bastar and Dharwar cratons, Peninsular India," *Gondwana Res.*, vol. 20, no. 2–3, pp. 335–343, 2011.

[3] A. M. Goodwin, *Precambrian geology: the dynamic evolution of the continental crust*. Elsevier, 1991.

[4] J. J. W. (John J. W. Naqvi, S. Mahmood, Rogers, *Precambrian geology of India*. Oxford University Press,Clarendon Press, 1987.

[5] M. E. A. Mondal, J. N. Goswami, M. P. Deomurari, and K. K. Sharma, "Ion microprobe 207Pb/206Pb ages of zircons from the Bundelkhand massif, northern India: Implications for crustal evolution of the Bundelkhand-Aravalli protocontinent," *Precambrian Res.*, vol. 117, no. 1–2, pp. 85–100, 2002, doi: 10.1016/S0301-9268(02)00078-5.

[6] K. B. Joshi *et al.*, "The diversification of granitoids and plate tectonic implications at the archaean-Proterozoic boundary in the bundelkhand craton, central India," *Geol. Soc. Spec. Publ.*, vol. 449, no. 1, pp. 123–157, 2017, doi: 10.1144/SP449.8.

[7] V. K. Singh and A. Slabunov, "The Central Bundelkhand Archaean greenstone complex, Bundelkhand craton, central India: Geology, composition, and geochronology of supracrustal rocks," in *International Geology Review*, Bellwether Publishing, Ltd., Sep. 2015, pp. 1349–1364. doi: 10.1080/00206814.2014.919613.

[8] J. K. Pati *et al.*, "Geology and geochemistry of giant quartz veins from the Bundelkhand Craton, central India and their implications," *J. Earth Syst. Sci.*, vol. 116, no. 6, pp. 497–510, 2007, doi: 10.1007/s12040-007-0046-y.

[9] K. G. Cox, J. D. Bell, and R. J. Pankhurst, "The Interpretation of Igneous Rocks George Allen and Unwin," *London, United Kingdom, 450p*, 1979.

[10] R. W. Le Maitre *et al.*, "Igneous rocks," *A Classif. Gloss. terms*, vol. 2, 2002.

[11] J. A. Winchester and P. A. Floyd, "Geochemical discrimination of different magma series and their differentiation products using immobile elements," *Chem. Geol.*, vol. 20, no. C, pp. 325–343, 1977, doi: 10.1016/0009-2541(77)90057-2.

[12] K. G. Cox, J. D. Bell, and R. J. Pankhurst, *The Interpretation of Igneous Rocks*. 1979. doi: 10.1007/978-94-017-3373-1.

[13] R. W. Le Maitre *et al.*, "A classification of

igneous rocks and glossary of terms. Recommendations of the IUGS Subcommission on the Systematics of Igneous rocks." Blackwell, Oxford, 1989.

[14] T. N. J. Irvine and W. R. A. Baragar, "A guide to the chemical classification of the common volcanic rocks," *Can. J. Earth Sci.*, vol. 8, no. 5, pp. 523–548, 1971.

[15] W. F. McDonough, S. S. Sun, A. E. Ringwood, E. Jagoutz, and A. W. Hofmann, "Potassium, rubidium, and cesium in the Earth and Moon and the evolution of the mantle of the Earth," *Geochim. Cosmochim. Acta*, vol. 56, no. 3, pp. 1001–1012, 1992, doi: 10.1016/0016-7037(92)90043-I.

[16] N. Nakamura, "Determination of REE, Ba, Fe, Mg, Na and K in carbonaceous and ordinary chondrites," *Geochim. Cosmochim. Acta*, vol. 38, no. 5, pp. 757–775, 1974, doi: 10.1016/0016-7037(74)90149-5.

[17] C. Rogers *et al.*, "Geochemistry and U-Pb geochronology of 1590 and 1550 Ma mafic dyke swarms of western Laurentia: Mantle plume magmatism shared with Australia," *Lithos*, vol. 314–315, pp. 216–235, 2018, doi: 10.1016/j.lithos.2018.06.002.

[18] B. CABANIS and M. LECOLLE, "Le diagramme La/10-Y/15-Nb/8: un outil pour la discrimination des séries volcaniques et la mise en évidence des processus de mélange et/ou de contamination crustale," *Comptes rendus l'Académie des Sci. Série 2, Mécanique, Phys. Chim. Sci. l'univers, Sci. la Terre*, vol. 309, no. 20, pp. 2023–2029, 1989.

[19] M. Meschede, "A method of discriminating between different types of mid-ocean ridge basalts and continental tholeiites with the Nb1bZr1bY diagram," *Chem. Geol.*, vol. 56, no. 3–4, pp. 207–218, 1986, doi: 10.1016/0009-2541(86)90004-5.

[20] J. A. Pearce and M. J. Norry, "Petrogenetic Implications of Ti, Zr, Y, and Nb Variations in Volcanic Rocks," 1979.

[21] H. R. Rollinson, *Using Geochemical Data: Evaluation, Presentation, Interpretation*. 1993. doi: 10.4324/9781315845548.

[22] J. W. Shervais, "TiV plots and the petrogenesis of modern and ophiolitic lavas," *Earth Planet. Sci. Lett.*, vol. 59, no. 1, pp. 101–118, 1982, doi: 10.1016/0012-821X(82)90120-0.